Gómez-Hernández, VJ.; Santos, AJ.; Blanco, E.; Lacroix, B.; García, R.; Huffaker, DL.; Morales, FM. (2019). Porosity Control for Plasma-Assisted Molecular Beam Epitaxy of GaN Nanowires. Crystal Growth & Design. 19(4):2461-2469. https://doi.org/10.1021/acs.cgd.9b00146

Porosity control for Plasma-Assisted Molecular Beam Epitaxy of GaN nanowires

Víctor J. Gomez[1]†, Antonio J. Santos[2,3], Eduardo Blanco[2,4], Bertrand Lacroix[2,3], Rafael García[2,3], Diana L. Huffaker[1,5], Francisco M. Morales[2,3]*

**Author to whom correspondence should be addressed.*

1 School of Engineering, Cardiff University, CF24 3AA, Cardiff, United Kingdom

2 IMEYMAT: Institute of Research on Electron Microscopy and Materials, University of Cádiz, Cádiz, Spain

3 Department of Materials Science and Metallurgic Engineering, and Inorganic Chemistry, Faculty of Sciences, University of Cádiz, 11510 Puerto Real, Cádiz, Spain

4 Department of Condensed Matter Physics, Faculty of Sciences, University of Cádiz, 11510 Puerto Real, Cádiz, Spain

5 School of Physics and Astronomy, Cardiff University, CF24 3AA, Cardiff, United Kingdom

KEYWORDS: III-Nitrides, Nanowires, Epitaxy, TEM, Ellipsometry.

ABSTRACT

We report on the bottom-up fabrication, by plasma-assisted molecular beam epitaxy, of monocrystalline GaN solid, hollow, and c-shape nanowires deposited in a compact fashion. The shape exhibited by these nanostructures varies from solid to c-shape and hollow nanowires. They were epitaxially grown with their [0001] directions perpendicular with respect to different surfaces of Si substrates. Advanced studies of these GaN nanostructures were carried out by means of selected-area electron diffraction, and scanning and high-resolution transmission electron microscopy evidencing their structure and epitaxial alignments with respect to the silicon. Through a comprehensive analysis of the growth conditions (substrate temperature and Ga and N* fluxes) we demonstrate that a local Ga-limited regime is the mechanism behind the particular shape of these nanostructures. Additionally, spectroscopic ellipsometry studies, applying a model based on Bruggeman effective medium approximations and taking into account several aspects related to the nature of these GaN nanostructures, were carried out to obtain valuable information about the evolution of the optical constants and the porosity along the layer. This work shows a way to control the porosity and shape of GaN nanowires by varying the growth conditions, which could open new horizons in the development of GaN nanostructures for future applications.

INTRODUCTION

Research on GaN nanostructures, such as nanowires (NWs) and nanoporous films (NPFs), has attracted substantial interest thanks to their high surface-to-volume ratio, and, in case of NWs, their strain-free nature[1]. The attractiveness of GaN NPFs resides in their significant strain relaxation[2,3], and enhanced surface Raman scattering[4]. Comparing with their compact counterparts, GaN NPFs have demonstrated improved properties in diverse applications such as photoelectrochemical water splitting[5,6,7], supercapacitors for energy storage[8,9], light emitting diodes (LEDs)[2,3,10,11,12,13], distributed Bragg reflectors[11], or mechanic removal of films from the substrate[14,15]. The research on NPFs is not limited to GaN: different materials such as nanoporous InGaN[16–19], Si[20], carbon membranes[21], and WO_3[22] have demonstrated a great potential for photoelectrochemical water splitting[18,20,21] and photocatalytic fuel cells[22].

A vast majority of reports on the synthesis of NPFs are focused on different kind of etching of thin films or GaN-sapphire templates such as electroless etching [3,4], electrochemical etching[6,10,17], or high temperature annealing[8,9]. The fabrication of ordered NPFs has been demonstrated using inductively coupled plasma (ICP) etching with an anodic alumina template as etching mask[23]. However, up to the best of our knowledge very few reports on the growth of GaN NPFs can be found. Recently, Aguilo and co-workers reported the growth of GaN NPFs by chemical vapor deposition[13] and its application on LEDs. The main drawbacks of the etching (top-down) approach are the difficulties of controlling the porosity level and shapes on the films. Therefore, a way to produce high-quality NPFs in a bottom-up approach with direct control over the composition, porosity and shape as well as low-cost routes to scale it to large areas for industrial transfer would be highly desirable.

In this paper, we present the growth of high-quality single crystalline GaN self-assembled NWs by plasma-assisted molecular beam epitaxy (MBE). GaN nanostructures were synthesized in a closed-packed manner that emulates the behavior of a NPF, combining the advantages offered by GaN NWs with the technological attractiveness of NPFs. The shape of the grown nanostructures varies from solid (SNW) to c-shape (CNW) and hollow (HNW) nanowires. By means of transmission electron microscopy (TEM) we show that wurtzite GaN S-, C- and H- NWs are grown along the [0001] direction, and epitaxially aligned with the underlying Si substrate. We demonstrate that a Ga-limited growth regime at the tips of the nanostructures is the mechanism behind their particular shapes. Consequently, we show control over the amount of porosity by tuning of the growth conditions. The porosity level is assessed through a comprehensive analysis of their optical properties by means of spectroscopic ellipsometry (SE).

EXPERIMENTAL SECTION

All studied samples were grown on chemically cleaned p-type Si (111) or (100) substrates in a Veeco Gen930 molecular beam epitaxy (MBE) reactor equipped with a radio frequency nitrogen plasma source and a sumo Knudsen effusion cell for Ga. The substrates employed were (111) ± 0.5º and (001) ± 0.5º oriented, single side polished and prime grade manufactured by Sil'Tronix®. Before transferring into the growth chamber, the substrates were outgassed at 250 ºC during 12 hours. Prior to growth, the Si substrates were heated in the growth chamber to 900 ºC for 30 minutes in order to remove the native oxide. The temperature was then slowly decreased (5 ºC/min) until a clear 7x7 surface reconstruction was observed (860 ºC) at the reflection high-energy electron diffraction (RHEED) pattern[24]. Then, the substrates were intentionally nitridated by exposing the surface to active nitrogen at 860 ºC during 10 minutes under $\phi_{N*} =$

$14x10^{14}\ {}^{at}/_{cm^2 s}$ generating a 2 nm thick β-Si_3N_4 layer (Figure S1 supplementary material). The growth conditions for the samples can be found in Table I.

	Impinging fluxes ($x10^{14}$ at.cm^{-2}.s^{-1})			
Sample	Ga	N*	T_{subs} (ºC)	Substrate
T1	8	11	800	Si(111)
T2	8	11	825	Si(111)
T2’	8	11	825	Si(100)
T3	8	11	850	Si(111)
G1	4	11	825	Si(111)
G3	10	11	825	Si(111)
N1	11	11	850	Si(111)
N2	11	14	850	Si(111)
N3	11	19	850	Si(111)
N4	11	22	850	Si(111)
N5	11	27	850	Si(111)

Table 1. Growth conditions for the samples referred in this study.

The surface morphology and sample thickness were assessed by means of scanning electron microscopy (SEM) using a Zeiss Gemini 1540XB SEM microscope. For the transmission electron microscopy (TEM) analyses, the samples were prepared in cross-sectional (XTEM) and plain-view (PVTEM) orientations and thinned to electron transparency by tripod mechanical polishing followed by Ar^+ ion milling at 3.5 keV, ±7º incidence with a PIPS system from GATAN. The

high-resolution TEM (HRTEM) and selected area electron diffraction (SAED) results were collected in a JEOL 2100 microscope equipped with a LaB_6 filament at an electron accelerating voltage of 200 kV. The energy dispersive x-ray spectra (EDS) and high-angle annular dark-field (HAADF) images were acquired using a FEI Talos F200S TEM operated in scanning TEM (STEM) mode. A variable angle spectroscopic ellipsometer equipped with an automatic rotating analyzer (J.A. Woollam V-VASE) was used to measure the ellipsometric angles, amplitude ratio (Ψ) and phase difference (Δ) between the reflected polarized light p and s components, at different angles of incidence, in the range of 0.5-5 eV. The samples' back surfaces had been previously scratched, so as to avoid incoherent back-surface reflection.

RESULTS AND DISCUSSION

Samples T2 and T2' were chosen for the morphological and structural analysis. Both samples were grown with the same conditions but on different substrates, Si(111) for sample T2 and Si(100) for T2'. Figures 1a and 1b show a cross-section SEM micrograph of samples T2 and T2', respectively, taken with an inclination of 15º, which exhibit a high density of nanostructures with an average height of (667 ± 17) and (734 ± 8) nm, diameters of (120 ± 5) and (134 ± 5) nm, and wall thicknesses of (16 ± 1) and (19 ± 1) nm, for samples T2 and T2' respectively. It can also be appreciated that these columnar nanostructures are grown straight and parallel to the surface normal direction on both substrates. The top morphology of these specimens is a combination of solid NWs (SNWs) with well-developed hexagonal facets, most likely m-planes (density on samples T2 and T2' ~ $4x10^8$ and $1x10^8$ cm^{-2}), hollow NWs (HNWs) with a hexagonal to dodecagonal shape, most likely a mixture of m- and a-planes (~ $3x10^8$ and $2x10^8$ cm^{-2}), and c-shape NWs (CNWs, ~ $3x10^9$ cm^{-2} on both samples). The different nanostructures are illustrated on the top-view SEM micrograph of samples T2 (figure 1c) and T2' (figure 1d). HAADF-XTEM

studies were carried out on sample T2 to elucidate up to which extent the nanostructures are hollow or solid. As can be seen from figure 1e, the highlighted CNW seems to be a kind of rolled film partially opened longitudinally. The great contrast between what we consider external and internal walls, make us think that these NWs are hollow. Note that the intensity on the HAADF images is proportional to the product of the effective atomic mass (the higher, the brighter) and the quantity of projected material. Considering pure GaN (see supporting info section 2 for energy dispersive x-ray spectroscopy, EDS) and that tripod polishing gives lamellae very uniform in width, then, different intensities are directly related with the local emptiness or compactness of the nanostructure. On figure 1f a brighter nanostructure with more homogeneous contrast can be observed (highlighted on the left side of this figure), so according to the previous explanation, it is most-likely a SNW. In addition, it can be appreciated an increased intensity at the base of the nanostructures (black dashed rectangle on figure 1f) than at the tips, suggesting that there is more GaN material on the bases of the nanostructures (closer to the substrate) than at the tips of the HNWs and CNWs. Analysis of the intensity of the HAADF-XTEM micrograph of sample T2 (figure S3 on the supporting info) confirms the intensity decrease with increasing the distance from the substrate. This fact, combined with the observed and commented NWs-type surface densities, support the idea that most of the uncompact NWs are actually composed by solid bases (or initially SNWs) that evolve some of them into hollow or most of them into c-shape structures as the growth proceeds (figure S4).

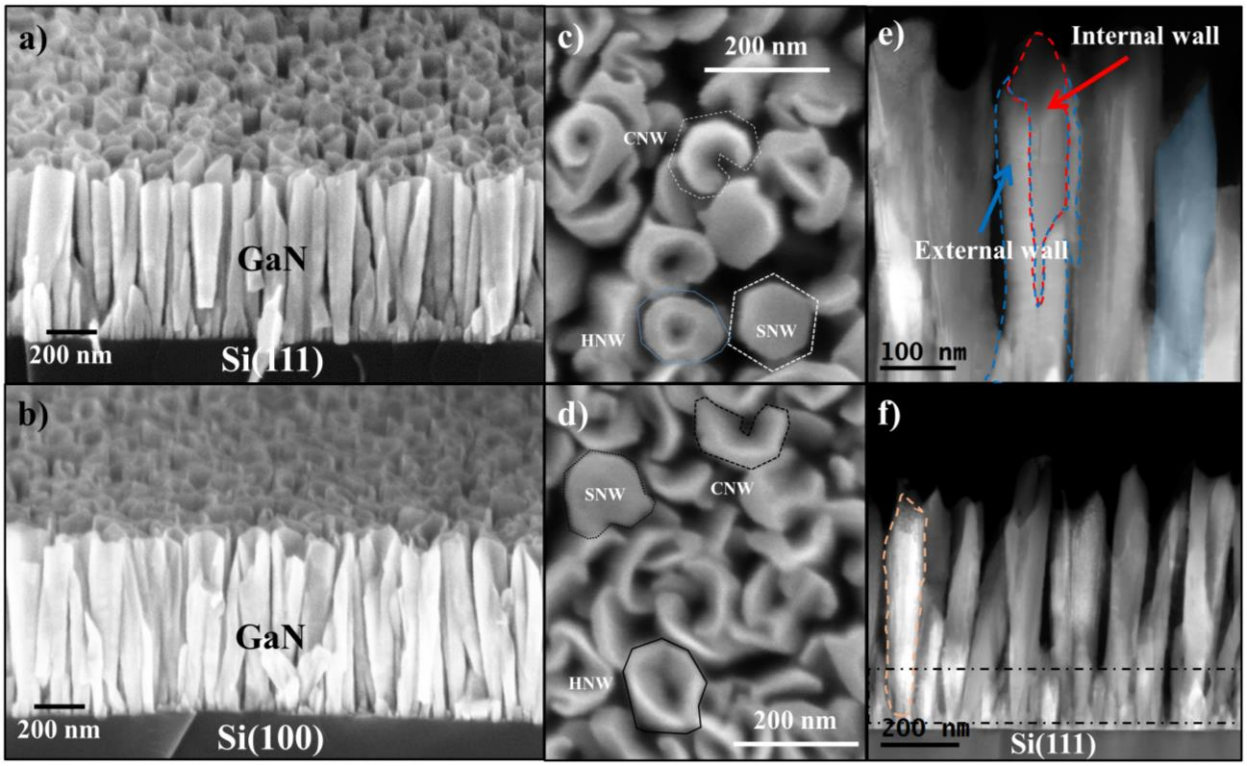

Figure 1. Cross-sectional SEM micrographs of a) sample T2 and b) sample T2' taken at an inclination of 15º, and parallel to the Si {110} cleavage edge. Top-view SEM micrograph of sample c) T2 and d) T2' that illustrates the morphology of the SNWs, HNWs and CNWs. e) and f) HAADF-XTEM micrographs of the GaN nanostructures taken along the [11$\bar{2}$0] GaN zone axis on sample T2: Dashed lines around internal (red) and external (blue) walls of a CNW, a brighter SNW (light orange) and GaN nanostructures bases (dashed-black rectangle) are included for clarity.

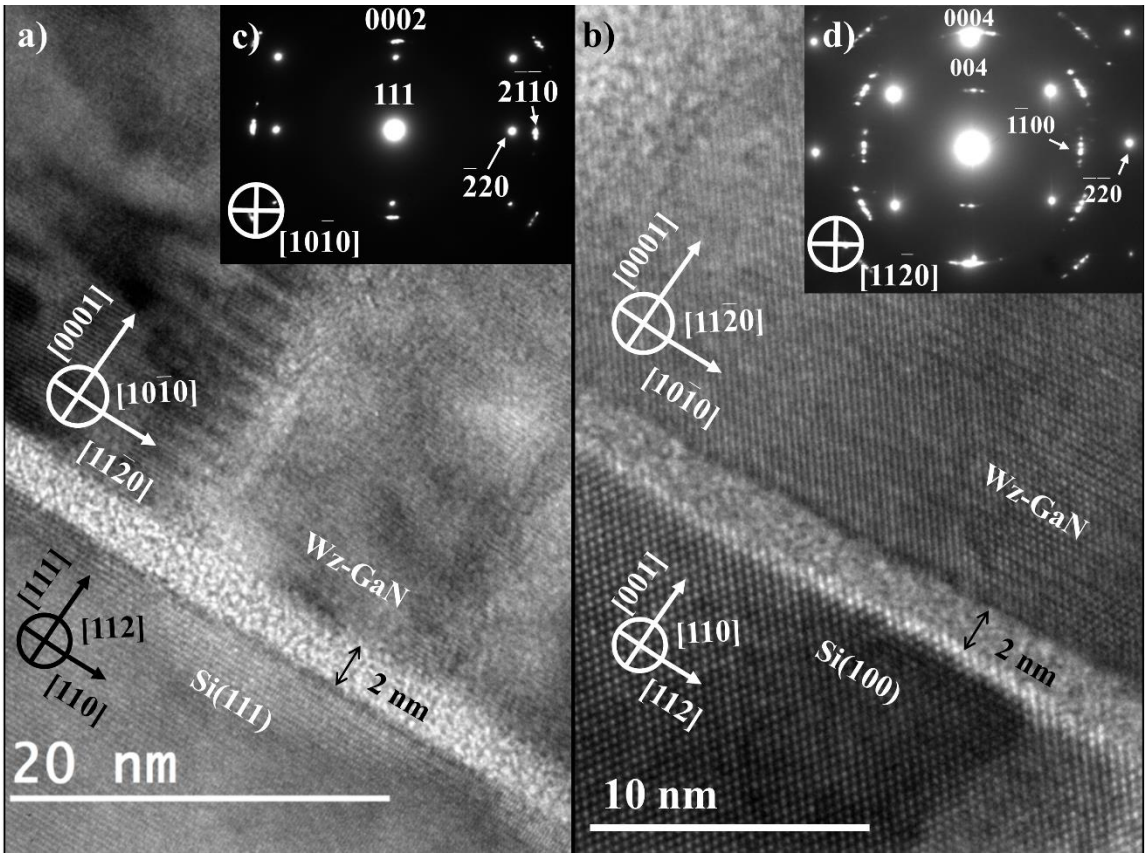

Figure 2. Cross-section HR-TEM images of GaN nanostructures on a) Si(111) (sample T2) along the [10$\bar{1}$0] zone axis and b) Si(100) (sample T2') along the [11$\bar{2}$0] zone axis. Both micrographs show an amorphized 2 nm thick β-Si_3N_4 interlayer. SAED patterns acquired over c) Sample T2 along the [10$\bar{1}$0] zone axis and d) sample T2' along the [11$\bar{2}$0] zone axis. Relevant reflections are marked for clarity on certain diffraction spots of both SAED patterns. Probing diameter of ~700 nm on both SAED patterns.

To probe the microstructure of the rods, we performed HR-XTEM experiments on samples T2 and T2' (figures 2a and 2b), along the [10$\bar{1}$0] and the [11$\bar{2}$0] GaN directions respectively, close to the interfaces among Si, β-Si_3N_4 and GaN. The nitridation technique explained in the experimental section gives rise to a 2 nm thick β-Si_3N_4 in both cases. The nanostructures are revealed to be

single-crystalline wurtzite GaN. According to figure 2a and 2b the GaN nanostructures grow with the c-axis perpendicular to the Si(111) and Si(100) planes. This observation concurs with SEM micrographs shown above (figures 1a and 1b). For the samples grown on Si(111) it also coincides with results reported by other groups[25–27]. In the case of Si(100) substrates, NWs grown with the c-direction perpendicular to the Si(100) plane agrees with previously reported results[26,28]. However, Shetty and co-workers reported similar mixture of nanostructures grown on Si(100)[29] with different alignment. They were tilted between 10° and 45° with respect to the Si(100) plane normal. In order to inspect the general epitaxial alignment between the GaN nanostructures and the underlying Si substrates in our specimens, SAED patterns, for more extended interface regions than those inspected by HRTEM, were collected (figures 2c and 2d). The diffraction spots related to GaN are arced due to the presence of a small tilt among the nanostructures (smaller for sample T2). A slight twist of some NWs with respect to surface normal cannot be disregarded, against a perfect heteroepitaxy, since only (0001) fringes are resolved on the GaN when the Si atomic columns are perfectly aligned with the electron-beam, and thus, resoluble by phase-contrast. Nevertheless, the SAED patterns reveals a general coherency between surface and nanowires lattices, then the epitaxial relationship is defined as GaN(0001)||Si(111) and GaN($10\bar{1}0$)||Si(112) for GaN on Si(111), and GaN(0001)||Si(001) and GaN($11\bar{2}0$)||Si(110) for GaN on Si(100). Moreover, this is the commonly reported epitaxial alignment for III-Nitrides (thin films and NWs) on Si(111)[25,27,30,31].

To gain deeper insight on the microstructure of the GaN rods we performed HR-PVTEM on a single SNW (Figure 3a and 3b) and a single CNW (figure 3d). The top-view of the SNW reveals a single crystalline GaN structure (confirming the observations done in figure 2a) with a hexagonal symmetry of atomic columns projected along the [0001] direction. The SNW shows a well-

developed hexagonal shape with $\{10\bar{1}0\}$ side facets. In the case of the CNW (Figure 3d), the micrograph reveals a single crystalline CNW with 5 well developed external side facets (most likely $\{10\bar{1}0\}$ facets) together with a 6^{th} opened one, forming an open hexagon. The internal facets are parallel to the external $\{10\bar{1}0\}$ side facets. In this specific case the wall thickness is (30.1 ± 0.5) nm. Insets of figures 3b and 3d are the fast Fourier transform (FFT), equivalent to a diffractogram, of the HR-TEM images of the SNW and the CNW, respectively. Both FFT images indicate a 6-fold symmetry, finger-print of the wurtzite crystal structure in polar direction, on both kind of nanostructures.

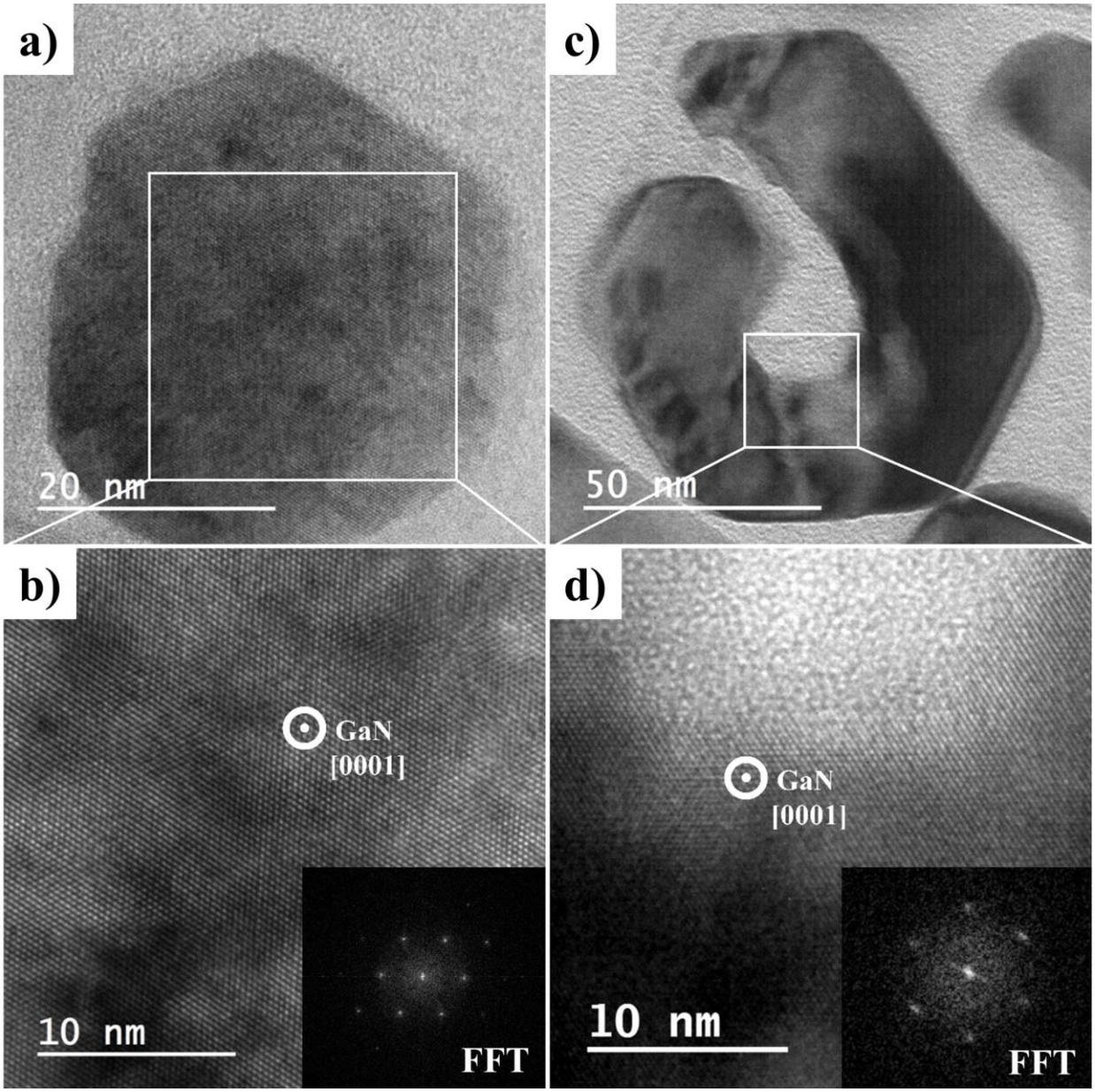

Figure 3. Top-view HR-PVTEM micrographs of a SNW a) and enlarged area in b), and a CNW c) and enlarged area in d) taken along the [0001] GaN zone axis. FFT images of both shown top-view HR-TEM micrographs of the SNW and the CNW are shown in their respective inset.

The natural question arising now is: what is the mechanism behind the formation of HNWs and CNWs? Three different explanations can be found in the literature for the spontaneous formation

of such structures: I.- The screw dislocation driven model[29,32]. II.- The reduction of the nucleation barrier along the NW top facet boundary by introducing high Si-flux[33]. III.- The growth under a locally (on the tips) Ga-limited regime[7,34,35].

Morin and co-workers [32] reported on the spontaneous formation of ZnO nanotubes driven by screw dislocations. In addition, Shetty *et al* [29] found the role of screw dislocations to be crucial for the formation of the internal facets on the HNWs and CNWs. To investigate the role of screw-type dislocations on the shape of the nanostructures we carried out TEM studies in two-beam diffraction-contrast conditions with g = 0002. Dislocations with total or partial screw component were found in a very low percentage of the studied nanostructures (< 5%), suggesting that there should be another mechanism behind the formation of HNWs and CNWs. The second model proposed can be disregarded by the fact that no Si flux was employed during the growth of the present nanostructures, and the used temperatures cannot justify Si sublimation or out-diffusion from the substrate. However, it is worth mentioning that the morphology of the structures reported by Bolshakov and co-workers[33] is similar to the morphology exhibited by Samples #1 and #2. Regarding the third mechanism, we performed a comprehensive study of the growth conditions (substrate temperature and Ga and N* fluxes), and their influence on the morphology of the nanostructures seem to be clear as it will be presented hereafter.

To probe the role of the local growth regime, we need to identify the effect of the different parameters on the local growth conditions. Once identified, we can design proper experiments. The number of Ga atoms arriving to the tip of the nanostructure per unit of time and unit of area is given by:

$$\phi_{Ga}^{loc} = \phi_{Ga} + \phi_{Ga}^{diff} + \phi_{GaN}^{dec} - \phi_{Ga}^{des} \quad \text{Eq (1)}$$

Being ϕ_{Ga} the Ga flux arriving directly to the tip *i.e.* the flux effusing from the K-cell, ϕ_{Ga}^{diff} accounts for the Ga atoms diffused from the substrate to the side-walls and from the side-walls to the tip, ϕ_{GaN}^{dec} is the contribution from the decomposition of the nanostructure itself, leaving Ga atoms on the tip. It is defined as:

$$\phi_{GaN}^{dec} = C.exp\left\{-{}^{E_{dec}}/_{k_B T}\right\} \quad \text{Eq (2)}$$

Fernandez-Garrido and co-workers[36] reported $C = (2.4 \pm 0.2) \times 10^{29}\, {}^{at}/_{cm^2 s}$ to be the decomposition pre-exponential factor and E_{dec} the activation energy for the decomposition process, with values ranging from 3.1 to 3.6 eV[36].

And ϕ_{Ga}^{des} accounts for the evaporation of Ga from the tip, given by the expression:

$$\phi_{Ga}^{des} = \mathrm{A}\left(\phi_{Ga} + \phi_{Ga}^{diff} + \phi_{GaN}^{dec}\right).exp\left\{-{}^{E_{des}}/_{k_B T}\right\} \quad \text{Eq(3)}$$

Where A is the desorption pre-exponential factor and E_{des} the activation energy for the desorption process. Bruno and co-workers reported $E_{des} = (2.85 \pm 0.02)\, eV$ for Ga desorbing from GaN(0001) surface[37]. According to the empirical work of Brandt and co-workers[38] the activation energy for desorption is lower for the $\{0001\}$ planes than for the $\{10\bar{1}0\}$ planes. Therefore, it is expected a higher desorption rate on the top facets than on the side- and internal- walls. To modify the local conditions, we can alter directly i.- the total Ga atoms lost by adjusting the substrate temperature, ii.- the amount of arriving Ga atoms by varying the temperature of the Ga effusion cell and therefore, the impinging Ga flux (ϕ_{Ga}), and iii.- the quantity of impinging N* atoms by tuning the plasma conditions (power or flux of pure N_2).

Effect of the substrate temperature: The variation of the substrate temperature has a direct effect on the amount of Ga desorbed from the surface and on the GaN decomposed. Note that the decomposition of GaN leaves liquid Ga on the surface that can be either reincorporated to the lattice with the excess of N* or desorbed from the surface. Figure 4 (a1 - a3) shows the effect of the growth temperature, from a nanowall network grown (figure a1) at 800 ºC to a low density packed SNWs at 850 ºC (figure 4a3). Figure 4c illustrates the density of the nanostructures with respect to the substrate temperature. A further reduction of the substrate temperature will reduce the Ga losses increasing the Ga available on the surface, therefore, promoting a more compact growth. At temperatures above 850 ºC the losses will become higher thus, resulting in no growth.

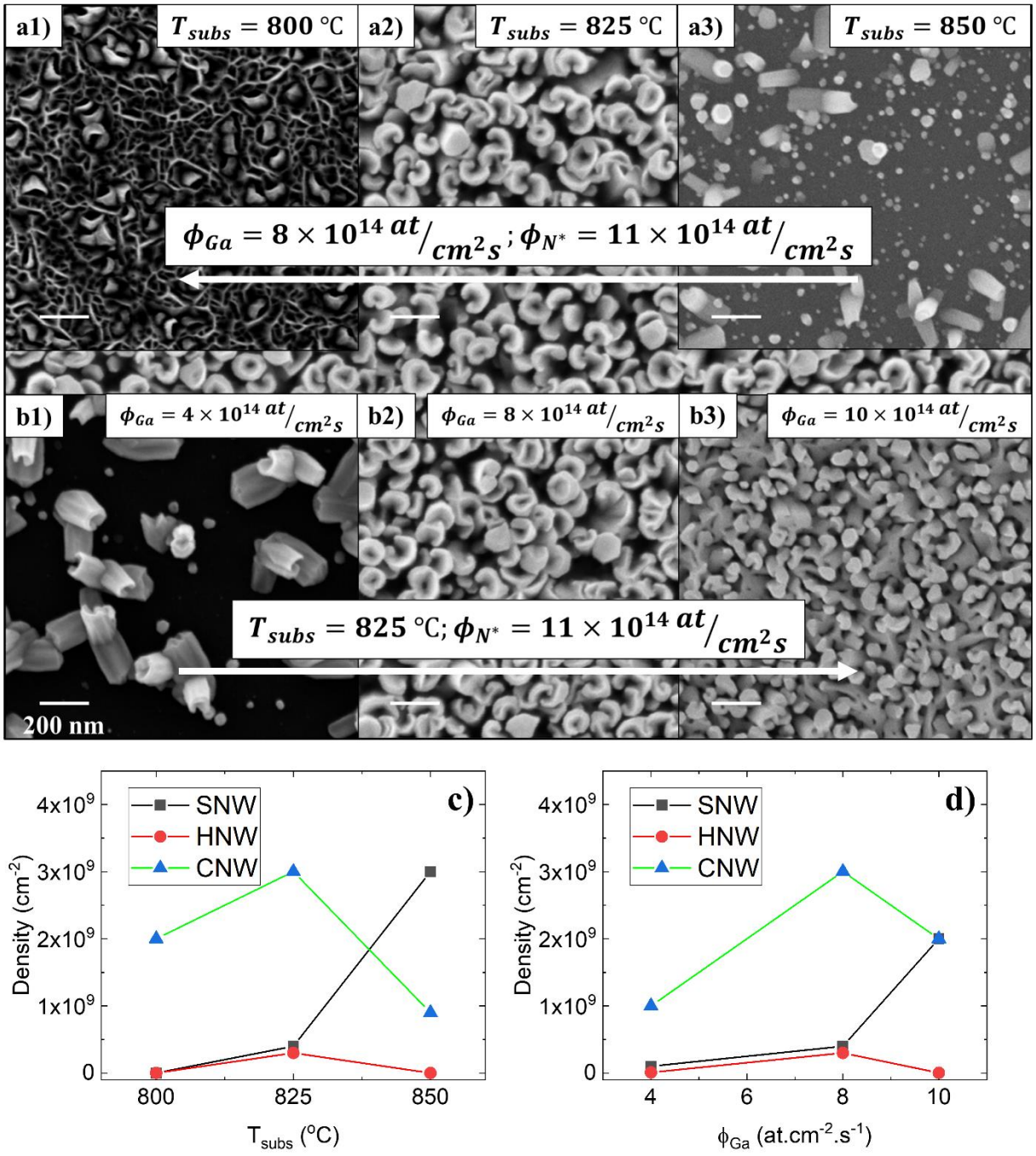

Figure 4. Top view SEM micrographs of GaN nanostructures grown on Si(111) at different substrate temperatures (Sample T1 – figure a1, T2-a2, and T3-a3) and different impinging Ga flux (ϕ_{Ga}) (Sample G1 – figure b1, T2-a2 and b2, and G3-b3). The white arrow points towards higher

temperatures or ϕ_{Ga}^{loc} values, respectively. Parameters kept constant are indicated over the white arrows. Density of the different nanostructures vs c) substrate temperature and d) ϕ_{Ga}. All the micrographs share a 200 nm scale bar. Note that micrographs a2 and b2 are the same.

Effect of the impinging Ga flux (ϕ_{Ga}): The variation of the impinging Ga flux has a direct effect on the amount of Ga arriving to the tip of the nanostructures. Figure 4 (b1 - b3) shows the results of the variation of the Ga flux. By increasing the ϕ_{Ga}, the amount of Ga atoms arriving to the tip of the nanostructures is increased modifying the local growth conditions. At the lowest ϕ_{Ga} (Figure 4 b1) the surface is characterized by the presence of doublets and triplets of CNWs (nanostructures with a common origin). At this condition Ga is the limiting reactant and the nanostructures are mainly of the CNW type. An increase in the amount of Ga reaching the sample results first in an increase on the density of nanostructures covering the surface, being dominant the HNW and CNW type, and, by further increasing, evolving to a more compact network of SNW. This variation on the density of the nanostructures as a function of the ϕ_{Ga} value is plotted on figure 4d.

Effect of the N* flux: The variation of the pure N_2 flux has a direct effect on the amount of active nitrogen arriving to the surface and hence the top of the nanostructures. Figure 5a shows the effect of increasing the active nitrogen flux. At the lowest ϕ_{N^*} (Figure 5a1) there is not enough N* overpressure to counteract the effects of the GaN decomposition and Ga desorption, resulting in a very low density of nanostructures. As the ϕ_{N^*} increases the surface is first saturated with nanostructures (Figure 5a2) and then, by further increasing the ϕ_{N^*}, CNWs become dominant over the SNWs (Figure 5 a3 to a5). The length of the nanostructures increases with the ϕ_{N^*} until it saturates at $\phi_{N^*} = 19 \times 10^{14}\ {}^{at}/_{cm^2.s}$, reaching the regime where Ga is the limiting reactant.

Once reached the Ga-limited regime the shape of the nanostructures is progressing from a majority of SNWs to a majority of CNWs, as it is demonstrated on figure 5b.

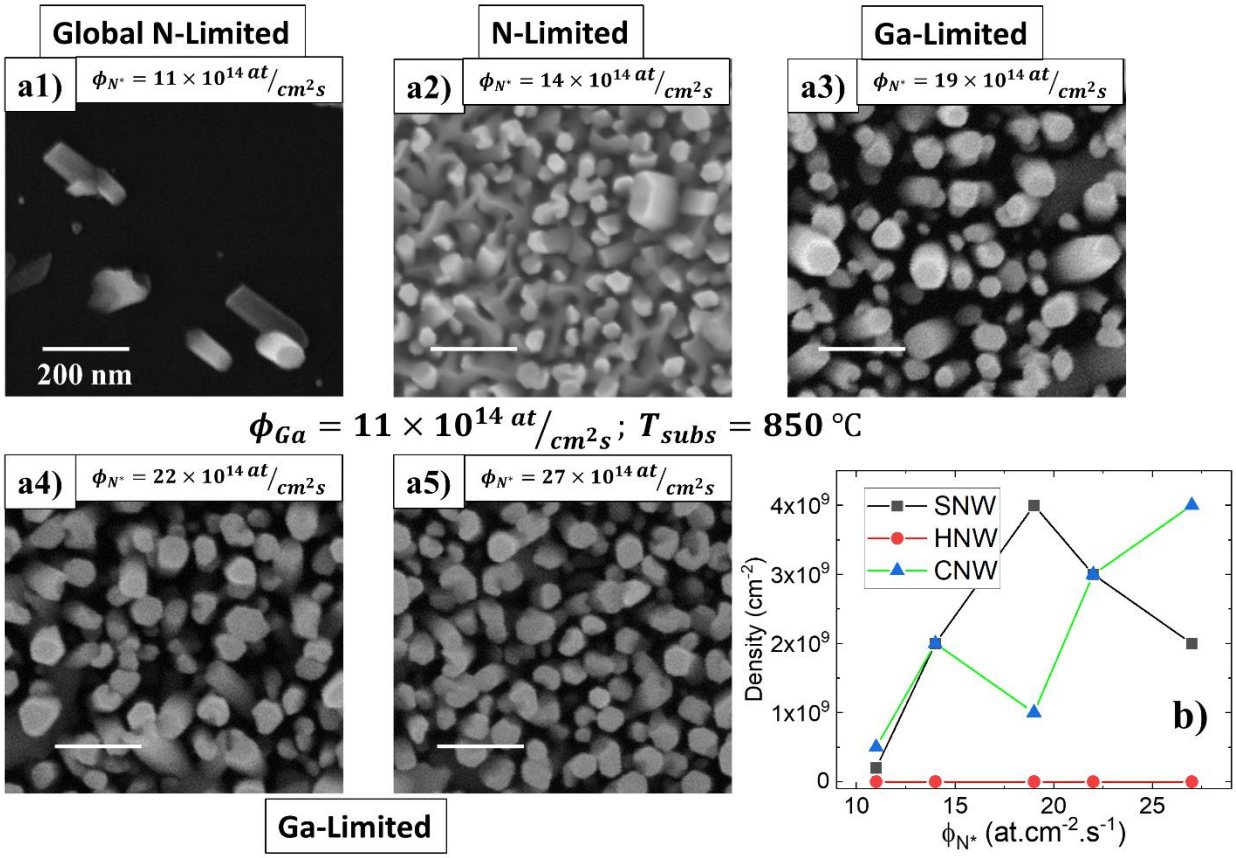

Figure 5. Top view SEM micrographs of GaN nanostructures grown on Si(111) for a1) – a5) different pure N_2 fluxes (samples N1 to N5). Parameters kept constant are indicated below figure a3. All the micrographs share a 200 nm scale bar. b) density of nanostructures vs pure N_2 flux.

Samples T3, G1 and N1 present a surface composed by a mixture of clusters, tilted NWs, tripods, tetrapods and multipods (Figures 4a3, 4b1 and 5a1). In the case of samples T3 and N1 the higher temperature (850 ºC) produces an increase in the GaN decomposition and Ga desorption rates impossible to stabilize with the given ϕ_{N^*}, whereas in the sample G1 the impinging Ga flux is directly reduced. In the self-assembled growth of nanowires two different regimes can be

distinguished; a nucleation phase, and a growth phase. The nucleation phase of GaN NWs is different than in standard crystal growth in the sense that GaN NWs do not nucleate directly in the form of wires. The nucleation phase comprises two successive periods: an initial incubation of stable nuclei in the form of clusters, followed by a transition period leading to shape transformations that eventually ends up with GaN NWs stable nuclei. During the growth phase the stable NWs nuclei grow axially and radially. The non-optimal growth conditions for those three samples affect primarily the nucleation phase, increasing the incubation time dramatically, and reducing the density of nuclei. During the transition period, and together with the limited incorporation of Ga into the crystal, the nuclei cannot reach the typical stable NW nuclei shape[39]. Thus, forming metastable nuclei with a non-conventional shape. During the subsequent growth phase, the metastable nuclei will elongate in the axial and radial directions and will end up in a mixture of tilted NWs, clusters, tripods, tetrapods and multipods in general (Figures 4a3, 4b1 and 5a1). The processes governing the particular shape of an individual NW are complex and out of the scope of this article. However, we think that it is a combination of the shape of any individual metastable nucleus, i.e. the particular orientation of their free surfaces, and the evaporation and reincorporation of the Ga atoms.

After the nucleation stage a stable NW nucleus is formed. Depending on the amount of Ga atoms with respect to the amount of N* arriving to the tip three different growth regimes can be distinguished:

When $\phi_{Ga}^{loc} = \phi_{N*}$ the growth proceeds in the axial direction with a negligible change in radius. This is the regime for growth of SNWs with flat top facet[39].

When $\phi_{Ga}^{loc} > \phi_{N*}$ the Ga atoms diffusing from the side-walls to the top facet get accumulated on the m-plane to c-plane edges and each NW starts growing radially as well as axially. The NW will continue increasing its radius until new equilibrium conditions are reached, self-regulating itself[40].

When $\phi_{Ga}^{loc} < \phi_{N*}$ three competing processes take place, the incorporation of Ga atoms on the top facet, the evaporation of Ga atoms from the top facet (c-plane) and side-walls (m-planes), and the incorporation of atoms on the m-plane to c-plane edges. According to the empirical work of Brandt and co-workers[38] the activation energy for desorption is lower for the $\{0001\}$ planes than for the $\{10\bar{1}0\}$ planes. Therefore, it is expected a higher desorption rate on the top facets than on the side-walls. Taking that into account, less Ga atoms are expected to remain on the top facet than on the side-walls. In addition to the direct flux coming from the k-cell, Ga atoms will diffuse from the side-walls to the top facet. When arriving to the top facet, the higher concentration of N*, as compared to the Ga concentration, will reduce the diffusion length of the Ga atoms promoting their incorporation on less favorable sites such as the m-plane to c-plane edges. As the growth proceeds, the Ga atoms continue to incorporate on the edges. It is worth mentioning that at the temperatures of those experiments the GaN decomposition rate is not negligible therefore, GaN is decomposed and Ga atoms can be either evaporate or reincorporate into the crystal. Under this conditions it is expected that the atoms incorporated on the edges will act as nucleation sites for the new arriving atoms. Thus, leaving a mixture of S-, H-, and C- NWs.

This comprehensive analysis of the shape of the nanostructures with respect to the growth conditions (growth temperature, ϕ_{Ga} and ϕ_{N^*}) demonstrates unambiguously that the mechanism behind their particular shape is the growth under local Ga-limited conditions. This mechanism has been pointed out to be behind the growth of ordered arrays of GaN nanotubes[34] on a Ti-masked

diamond substrate. In their case the local conditions on the tip were tuned by controlling the geometrical design of the mask (small period and large diameter). In addition, Park and co-workers[7] reported the growth of ordered arrays of GaN HNWs by MBE when using a low ϕ_{Ga}. Therefore, our findings are compatible with existing literature, provide an exhaustive growth map, and complement the already stablished theory on the growth of self-induced GaN NWs[1,39–41].

Spectroscopic ellipsometry analyses were performed on samples N3, N4 and N5 to find out the impact of growth under Ga-limited conditions on both the total porosity and the evolution of the optical constants along the GaN nanostructure in a larger scale. Herein, the term porosity will be defined as the percentage of air/voids in the GaN material. For reference, 0% porosity will be associated with a compact solid GaN thin film, composed by 100% GaN and 0% air.

Analyses were carried out considering a wavelength range from 250 to 2500 nm (5-0.5 eV) and the angles of incidence were varied between 55 and 75 degrees. The spot size of the light beam used was 3 mm which was always positioned in the central region of the sample. The depolarization was registered in all cases and it was included in the fitting process. As a first approach, the average porosity of each film was obtained by a pure Bruggeman effective medium approximation (BEMA) model, incorporating a mix of wurtzite GaN from the Woollam software library[42] and voids to describe the GaN nanowires layer, and assuming that individual nanowires exhibit the same behavior as the dense material. The calculated porosities show an increase of the voids proportion from 56% for sample N3 to 66% on sample N5 which could be associated with a boost in the density of CNWs.

Figure 6a shows the ellipsometric BEMA model enhanced by separating the in-plane (X, Y) and out-of-plane (Z) optical responses (uniaxial anisotropy). The out-of-plane depolarization factor

was fitted to $q_z \approx 0$, with the sum of q_x and q_y being the difference of q_z from 1, due to the columnar morphology (perpendicular to the substrate) of the nanostructures[43,44,45]. In order to reproduce the morphology of the GaN porous film, it was also assumed a variation in the refractive indexes (n) of the GaN nanostructure along the Z direction (a graded-index layer) so that it decreases, up to n=1 on the surface, as we move away from the substrate. Such variation is originated by internal changes in the structure of the nanowires rather than by modifications in the number of nanowires per surface unit. Furthermore, layer thickness non-uniformity was obtained from the depolarization registered during the experiments. Additionally, a 2 nm thin layer of silicon nitride (Si_3N_4), located between the substrate and the nanowire layer, was also considered in the optical model. Making all these considerations and fixing the porosity values obtained from the pure BEMA aforementioned, the defined model shows a good agreement for the modeled and the experimental spectra, obtaining good mean square errors (MSE) including depolarization (see supporting info figure S4 for the experimental and modeled ellipsometric measurements). Note that the thicknesses predicted by the model ((446 ± 0.24); (460 ± 0.50); (383 ± 0.25) for N3, N4 and N5 respectively) differ slightly from those measured by SEM ((402 ± 18); (385 ± 26); (367 ± 14) nm for N3, N4 and N5 respectively), being bigger for N3 and N4 samples. These differences could be related to the non-uniformity of thickness which in turn is responsible for the measured depolarization. This non-uniformity along the spot size reaches to the 18% for N3 sample, 22% for N4 and is significantly lower for sample N5 where it is 6%.

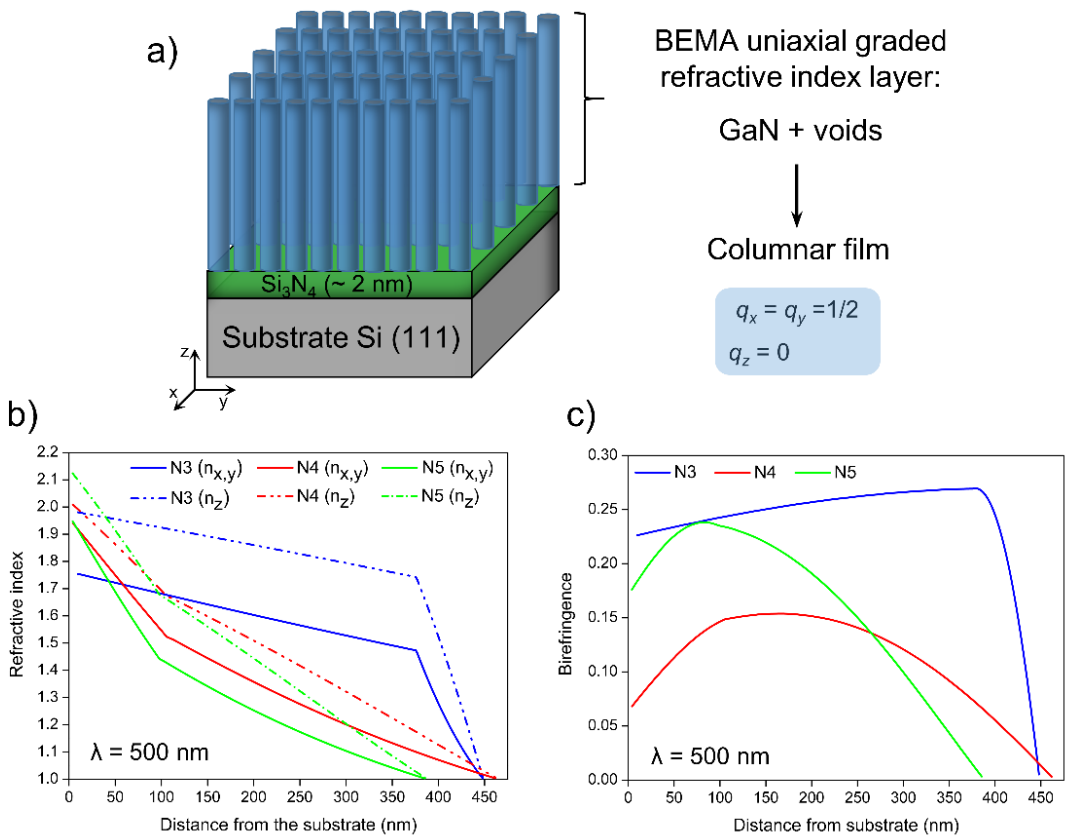

Figure 6. a) Ellipsometric BEMA model of the GaN nanowire film. b) In-plane (solid lines) and out-of-plane (dashed lines) refractive index and c) birefringence, $n_e - n_o$, evolution versus the position within the thickness of layer at 500 nm wavelength.

The results obtained from the BEMA model let us know some further information about the studied systems. First of all, it can be noted that GaN nanostructure layers have a high porosity, which leads to lower refractive indexes when compared to a massive GaN (see supporting info Figure S5 for refractive index vs. wavelength). Moreover, it can also be observed that this refractive index decreasing is more pronounced for greater N_2 fluxes which would demonstrate a direct correlation between the effect of the total density of nanostructures and the SNWs to CNWs proportion in the refractive index. Figure 6 (b-c) summarizes the evolution of the refractive index of uniaxial anisotropic GaN nanowire layers along the out-of-plane direction. Here can be found that the

refractive index in the Z direction is in all samples greater than those corresponding to the in-plane directions, being the difference between both (birefringence) stronger for lower total densities of NWs and higher concentrations of SNWs. It is important to highlight that N4 and N5 samples present a faster drop in *n* within the first 100 nm, which could be related to a structural change from SNWs to CNWs, *i.e.*, at the beginning all the NWs would have a solid base which could develop the c-shape or not depending on the growth conditions. This would be also in agreement with the aforementioned accumulation of material on the bases of these nanostructures. Therefore, taking this into account, it could be said that the concentration of CNWs is higher in N5 than in the N4 sample because the decrease of *n* is sharper in the region close to the substrate. By contrast to this, N3 sample exhibits a constant and softer *n* decrease except in the zone close to the surface, after 370 nm, which could be associated with the non-uniformity in thickness (18% in this case). This fact makes us think this last layer would be fundamentally composed of SNWs. Moreover, the low initial value of both $n_{x,y}$ and n_z in N3 sample is due to its smaller total density of NWs (see figure 5a3 and 5b).

CONCLUSIONS

In this paper we performed a thorough study of GaN-on-Si nanostructures growth by PAMBE. HR-TEM analysis showed single crystalline SNWs, HNWs and CNWs epitaxially aligned with the underlying Si substrate, and their effect on the morphology of the nanostructures. We have pointed out that the growth under local Ga-limited conditions is the mechanism behind the particular morphology of the nanostructures. Our findings are compatible with existing literature, provide an exhaustive growth map, and complement the already stablished theory on the growth

of self-induced GaN NWs. The porosity of the samples as well as the evolution of the optical constants along their thickness were obtained from the fitting of the ellipsometry measurements to the BEMA uniaxial model. By tuning the growth conditions, the density and shape of the nanostructures, and thus, the porosity can be controlled. The particular morphology of the samples presented in this article together with the demonstrated control over the porosity level will potentially open new horizons in the development of GaN nanostructures for future applications.

ASSOCIATED CONTENT

Supporting Information.

Intentional nitridation, compositional analysis, intensity analysis of HAADF-XTEM micrograph of sample T2, additional TEM micrographs C-NWs at their interface region with Si, and ellipsometry modeling of GaN nanoporous film (PDF).

AUTHOR INFORMATION

Corresponding Author

* Email: victor.gomez@ftf.lth.se

Present Addresses

† Present address: Solid State Physics, Lund University, Box 118, S-221 00 Lund, Sweden.

Author Contributions

The manuscript was written through contributions of all authors. All authors have given approval to the final version of the manuscript.

ACKNOWLEDGMENT

The authors would like to acknowledge the financial support provided by Sêr Cymru National Research Network in Advanced Engineering and Materials. V. J. Gomez acknowledge Dr P Caroff and Dr M. Kesaria for fruitful discussions. A. J. Santos would like to thank the IMEYMAT Institute and the Spanish Ministerio de Educación y Cultura for the concessions of grants (ICARO-173873 and FPU16-04386). The "Talent Attraction Program" of the University of Cádiz is acknowledged by supporting B. Lacroix contract code E-11-2017-0117214. University of Cádiz and IMEYMAT are also agreed by financing the mutual facilities available at the UCA R&D Central Services (SC-ICYT), the UCA project reference "PUENTE PR2018-040", and the IMEYMAT project reference "AGREGADOR 2018-1".

REFERENCES

(1) Knelangen, M.; Consonni, V.; Trampert, a; Riechert, H. In Situ Analysis of Strain Relaxation during Catalyst-Free Nucleation and Growth of GaN Nanowires. *Nanotechnology* **2010**, *21*, 245705.

(2) Vajpeyi, A. P.; Tripathy, S.; Chua, S. J.; Fitzgerald, E. A. Investigation of Optical Properties of Nanoporous GaN Films. *Phys. E Low-Dimensional Syst. Nanostructures* **2005**, *28*, 141–149.

(3) Najar, A.; Gerland, M.; Jouiad, M. Porosity-Induced Relaxation of Strains in GaN Layers Studied by Means of Micro-Indentation and Optical Spectroscopy. *J. Appl. Phys.* **2012**, *111*, 093513.

(4) Williamson, T. L.; Guo, X.; Zukoski, A.; Sood, A.; Díaz, D. J.; Bohn, P. W. Porous GaN as a Template to Produce Surface-Enhanced Raman Scattering-Active Surfaces. *J. Phys. Chem. B* **2005**, *109*, 20186–20191.

(5) Ryu, S. W.; Zhang, Y.; Leung, B.; Yerino, C.; Han, J. Improved Photoelectrochemical

Water Splitting Efficiency of Nanoporous GaN Photoanode. *Semicond. Sci. Technol.* **2012**, *27*, 015014.

(6) Benton, J.; Bai, J.; Wang, T.; Kingdom, U. Nanoporous GaN for Enhanced Solar Hydrogen Production. *Proc. SPIE* **2014**, *9176*, 91760.

(7) Park, J.; Mandal, A.; Kang, S.; Chatterjee, U.; Kim, J. S. Hydrogen Generation Using Non-Polar Coaxial InGaN / GaN Multiple Quantum Well Structure Formed on Hollow n-GaN Nanowires. *Sci. Rep.* **2016**, *6*, 31996.

(8) Zhang, L.; Wang, S.; Shao, Y.; Wu, Y.; Sun, C.; Huo, Q.; Zhang, B.; Hu, H.; Hao, X. One-Step Fabrication of Porous GaN Crystal Membrane and Its Application in Energy Storage. *Sci. Rep.* **2017**, *7*, 44063.

(9) Yu, J.; Zhang, L.; Shen, J.; Xiu, Z.; Liu, S. Wafer-Scale Porous GaN Single Crystal Substrates and Their Application in Energy Storage. *CrystEngComm* **2016**, *18*, 5149–5154.

(10) Lee, K. J.; Kim, S.-J.; Kim, J.-J.; Hwang, K.; Kim, S.-T.; Park, S.-J. Enhanced Performance of InGaN/GaN Multiple-Quantum-Well Light-Emitting Diodes Grown on Nanoporous GaN Layers. *Opt. Express* **2014**, *22*, A1164.

(11) Shiu, G. Y.; Chen, K. T.; Fan, F. H.; Huang, K. P.; Hsu, W. J.; Dai, J. J.; Lai, C. F.; Lin, C. F. InGaN Light-Emitting Diodes with an Embedded Nanoporous GaN Distributed Bragg Reflectors. *Sci. Rep.* **2016**, *6*, 29138.

(12) Hsu, W.-J.; Chen, K.-T.; Huang, W.-C.; Wu, C.-J.; Dai, J.-J.; Chen, S.-H.; Lin, C.-F. InGaN Light Emitting Diodes with a Nanopipe Layer Formed from the GaN Epitaxial Layer. *Opt. Express* **2016**, *24*, 11601.

(13) Carvajal, J. J.; Mena, J.; Aixart, J.; Díaz, F.; Aguiló, M. Rectifiers, MOS Diodes and LEDs Made of Fully Porous GaN Produced by Chemical Vapor Deposition. *ECS J. Solid State*

Sci. Technol. **2017**, *80*, 143–148.

(14) Huang, S.; Zhang, Y.; Leung, B.; Yuan, G.; Wang, G.; Jiang, H.; Fan, Y.; Sun, Q.; Wang, J.; Xu, K.; et al. Mechanical Properties of Nanoporous GaN and Its Application for Separation and Transfer of GaN Thin Films. *ACS Appl. Mater. Interfaces* **2013**, *5*, 11074–11079.

(15) Huo, Q.; Shao, Y.; Wu, Y.; Zhang, B.; Hu, H.; Hao, X. High Quality Self-Separated GaN Crystal Grown on a Novel Nanoporous Template by HVPE. *Sci. Rep.* **2018**, *8*, 1–8.

(16) Abud, S. H.; Hassan, Z.; Yam, F. K. Enhancement of Structural and Optical Properties of Porous In0.27Ga0.73N Thin Film Synthesized Using Electrochemical Etching Technique. *Int. J. Electrochem. Sci.* **2012**, *7*, 10038–10046.

(17) Radzali, R.; Hassan, Z.; Zainal, N.; Yam, F. K. Nanoporous InGaN Prepared by KOH Electrochemical Etching with Different Light Sources. *Microelectron. Eng.* **2014**, *126*, 107–112.

(18) Soto Rodriguez, P. E. D.; Nash, V. C.; Aseev, P.; Gómez, V. J.; Kumar, P.; Alvi, N. U. H.; Sánchez, A.; Villalonga, R.; Pingarrón, J. M.; Nötzel, R. Electrocatalytic Oxidation Enhancement at the Surface of InGaN Films and Nanostructures Grown Directly on Si(111). *Electrochem. commun.* **2015**, *60*, 158–162.

(19) Abud, S. H.; Hassan, Z.; Yam, F. K. Fabrication and Characterization of Metal-Semiconductor-Metal Photodetector Based on Porous InGaN. *Mater. Chem. Phys.* **2014**, *144*, 86–91.

(20) Xing, Z.; Ren, F.; Wu, H.; Wu, L.; Wang, X.; Wang, J.; Wan, D.; Zhang, G.; Jiang, C. Enhanced PEC Performance of Nanoporous Si Photoelectrodes by Covering HfO2 and TiO2 Passivation Layers. *Sci. Rep.* **2017**, *7*, 43901.

(21) Wang, H.; Min, S.; Ma, C.; Liu, Z.; Zhang, W.; Wang, Q.; Li, D.; Li, Y.; Turner, S.; Han, Y.; Zhu, H.; Abou-Hamad, E.; Hedhili, M. N.; Pan, J.; Yu, W.; Huang, K. W.; Li, L. J.; Yuan, J.; Antonietti, M.; Wu, T. Synthesis of Single-Crystal-like Nanoporous Carbon Membranes and Their Application in Overall Water Splitting. *Nat. Commun.* **2017**, *8*, 13592.

(22) Xia, L.; Bai, J.; Li, J.; Zeng, Q.; Li, X.; Zhou, B. A Highly Efficient BiVO4/WO3/W Heterojunction Photoanode for Visible-Light Responsive Dual Photoelectrode Photocatalytic Fuel Cell. *Appl. Catal. B Environ.* **2016**, *183*, 224–230.

(23) Wang, Y. D.; Chua, S. J.; Sander, M. S.; Chen, P.; Tripathy, S.; Fonstad, C. G. Fabrication and Properties of Nanoporous GaN Films. *Appl. Phys. Lett.* **2004**, *85*, 816–818.

(24) Suzuki, T.; Hirabayashi, Y. First Observation of the Si(111)-7 x 7<->1 x 1 Phase Transition by the Optical Second Harmonic Generation. *Jpn. J. Appl. Phys.* **1993**, *32*, L610–L613.

(25) Wierzbicka, A.; Zytkiewicz, Z. R.; Kret, S.; Borysiuk, J.; Dluzewski, P.; Sobanska, M.; Klosek, K.; Reszka, A.; Tchutchulashvili, G.; Cabaj, A.; Tchutchulashvili, G.; Cabaj, A.; Lusakowska, E. Influence of Substrate Nitridation Temperature on Epitaxial Alignment of GaN Nanowires to Si(111) Substrate. *Nanotechnology* **2013**, *24*, 035703.

(26) Calleja, E.; Ristić, J.; Fernández-Garrido, S.; Cerutti, L.; Sánchez-García, M. A.; Grandal, J.; Trampert, A.; Jahn, U.; Sánchez, G.; Griol, A.; Sánchez, B. Growth, Morphology, and Structural Properties of Group-III-Nitride Nanocolumns and Nanodisks. *Phys. Status Solidi Basic Res.* **2007**, *244*, 2816–2837.

(27) Gačević, Ž.; Bengoechea-Encabo, A.; Albert, S.; Torres-Pardo, A.; Gonzalez-Calbet, J. M.; Calleja, E. Crystallographically Uniform Arrays of Ordered (In) GaN Nanocolumns Crystallographically Uniform Arrays of Ordered (In) GaN Nanocolumns. *J. Appl. Phys.*

2015, *117*, 035301.

(28) Fan, S.; Shih, I.; Mi, Z. A Monolithically Integrated InGaN Nanowire / Si Tandem Photoanode Approaching the Ideal Bandgap Configuration of 1.75/1.13 EV. *Adv. Energy Mater.* **2017**, *7*, 1600952.

(29) Shetty, S.; Kesaria, M.; Ghatak, J.; Shivaprasad, S. M. The Origin of Shape, Orientation, and Structure of Spontaneously Formed Wurtzite GaN Nanorods on Cubic Si(001) Surface. *Cryst. Growth Des.* **2013**, *13*, 2407–2412.

(30) Gómez, V. J.; Gačević, Z.; Soto-Rodríguez, P. E. D.; Aseev, P.; Nötzel, R.; Calleja, E.; Sánchez-García, M. A. Comparative Study of Single InGaN Layers Grown on Si(111) and GaN(0001) Templates: The Role of Surface Wetting and Epitaxial Constraint. *J. Cryst. Growth* **2016**, *447*, 48–54.

(31) Dadgar, A.; Veit, P.; Schulze, F.; Bläsing, J.; Krtschil, A.; Witte, H.; Diez, A.; Hempel, T.; Christen, J.; Clos, R.; Krost, A. MOVPE Growth of GaN on Si - Substrates and Strain. *Thin Solid Films* **2007**, *515*, 4356–4361.

(32) Morin, S. A.; Bierman, M. J.; Tong, J.; Jin, S. Mechanism and Kinetics of Spontaneous Nanotube Growth Driven by Screw Dislocations. *Science* **2010**, *328*, 476–480.

(33) Bolshakov, A. D.; Mozharov, A. M.; Sapunov, G. A.; Shtrom, I. V.; Sibirev, N. V.; Fedorov, V. V.; Ubyivovk, E. V.; Tchernycheva, M.; Cirlin, G. E.; Mukhin, I. S. Dopant-Stimulated Growth of GaN Nanotube-like Nanostructures on Si(111) by Molecular Beam Epitaxy. *Beilstein J. Nanotechnol.* **2018**, *9*, 146–154.

(34) Schuster, F.; Hetzl, M.; Weiszer, S.; Garrido, J. A.; De La Mata, M.; Magen, C.; Arbiol, J.; Stutzmann, M. Position-Controlled Growth of GaN Nanowires and Nanotubes on Diamond by Molecular Beam Epitaxy. *Nano Lett.* **2015**, *15*, 1773–1779.

(35) Wei, P. C.; Chen, L. C.; Chen, K. H. Surface Diffusion Controlled Formation of High Quality Vertically Aligned InN Nanotubes. *J. Appl. Phys.* **2014**, *116*, 124301.

(36) Fernández-Garrido, S.; Koblmüller, G.; Calleja, E.; Speck, J. S. In Situ GaN Decomposition Analysis by Quadrupole Mass Spectrometry and Reflection High-Energy Electron Diffraction. *J. Appl. Phys.* **2008**, *104*, 033541.

(37) Bruno, G.; Losurdo, M.; Kim, T. H.; Brown, A. Adsorption and Desorption Kinetics of Ga on GaN(0001): Application of Wolkenstein Theory. *Phys. Rev. B - Condens. Matter Mater. Phys.* **2010**, *82*, 075326.

(38) Brandt, O.; Sun, Y. J.; Däweritz, L.; Ploog, K. H. Ga Adsorption and Desorption Kinetics on M-Plane GaN. *Phys. Rev. B - Condens. Matter Mater. Phys.* **2004**, *69*, 165326.

(39) Consonni, V. Wide Band Gap Semiconductor Nanowires 1: Low-Dimensionality Related Effects and Growth; Consonni, V., Feuillet, G., Baptist, R., Eds.; Wiley, 2014; pp 177–213.

(40) Kaganer, V. M.; Fernández-Garrido, S.; Geelhaar, L.; Calleja, E.; Sabelfeld, K. K.; Grandal, J.; Gotschke, T.; Brandt, O. Self-Regulated Radius of Spontaneously Formed GaN Nanowires in Molecular Beam Epitaxy. *Nano Lett.* **2013**, *13*, 3274–3280.

(41) Consonni, V.; Hanke, M.; Knelangen, M.; Geelhaar, L.; Trampert, A.; Riechert, H. Nucleation Mechanisms of Self-Induced GaN Nanowires Grown on an Amorphous Interlayer. *Phys. Rev. B - Condens. Matter Mater. Phys.* **2011**, *83*, 035310.

(42) Adachi, S. *Optical Constants of Crystalline and Amorphous Semiconductors*; Springer Science, Ed.; Springer, Boston, MA: Boston : Kluwer Academic Publishers, 1999.

(43) Kaminska, K.; Amassian, A.; Martinu, L.; Robbie, K. Growth of Vacuum Evaporated Ultraporous Silicon Studied with Spectroscopic Ellipsometry and Scanning Electron Microscopy. *J. Appl. Phys.* **2005**, *97*, 013511.

(44) Jones, S. B.; Friedman, S. P. Particle Shape Effects on the Effective Permittivity of Anisotropic or Isotropic Media Consisting of Aligned or Randomly Oriented Ellipsoidal Particles. *Water Resour. Res.* **2000**, *36*, 2821–2833.

(45) Gospodyn, J.; Sit, J. C. Characterization of Dielectric Columnar Thin Films by Variable Angle Mueller Matrix and Spectroscopic Ellipsometry. *Opt. Mater. (Amst).* **2006**, *29*, 318–325.

For Table of Contents Use Only

Porosity control for Plasma-Assisted Molecular Beam Epitaxy of GaN nanowires

Víctor J. Gomez[1]†, Antonio J. Santos[2,3], Eduardo Blanco[2,4], Bertrand Lacroix[2,3], Rafael García[2,3], Diana L. Huffaker[1,5], Francisco M. Morales[2,3]*

TOC Graphic:

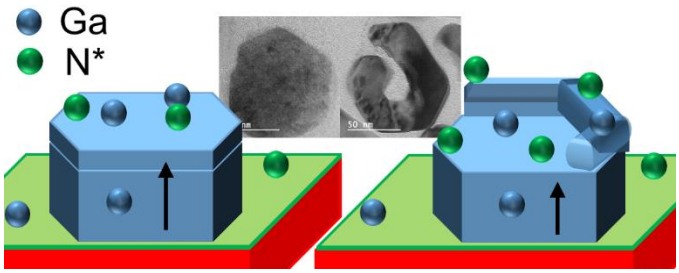

Synopsis:

We report on the morphology control of GaN nanowires grown by molecular beam epitaxy. Their shape varies from solid to c- and hollow nanowires. The nanostructures are characterized by selected-area electron diffraction, scanning and high-resolution transmission electron microscopy. The growth under a local Ga-limited regime is the mechanism behind their particular shape. The porosity is characterized by means of ellipsometry.